scientific reports

Check for updates

OPEN

Characterization of a phosphoinositide-binding protein containing a PHOX homology domain in the malaria parasite *Plasmodium falciparum*

Stéphanie Roucheray[1,2,3], Dominik Stastny[4], Harpreet Kaur[5], Dana Tahotna[4], Joel B. Dacks[5,6,7], Peter Griac[4] & Dave Richard[1,2,3]✉

Phosphoinositides (PIPs), are key regulators of membrane identity and vesicular trafficking. By dynamically shaping the lipid composition of intracellular membranes, PIPs help ensure the specificity of cargo delivery. In apicomplexan parasites such as *Plasmodium falciparum*, the biogenesis of the specialized secretory organelles involved in erythrocyte invasion (named rhoptries, micronemes, and dense granules), remains poorly understood, particularly regarding how proteins are sorted and specifically targeted to their respective destinations. Our hypothesis is that PIPs might play a role in this process. We here present our characterization of the *P. falciparum* protein Pf3D7_0704400, a putative PIP-binding protein containing a PX domain. We named this protein PfPX2, following the previously characterized PX domain-containing protein PfPX1. In silico structural analysis revealed that the PfPX2 PX domain contains both canonical and non-canonical PIP-binding motifs and a positively charged binding pocket. Lipid binding assays showed that the PfPX2 PX domain can bind all species of PIPs with a preference for PI3P, PI5P and PI(3,5)P2. Immunofluorescence assays demonstrated that PfPX2 localized to the Golgi apparatus and the micronemes in developing schizonts. Moreover, proximity labelling enabled the identification of protein such as PfSortilin, the clathrin heavy chain and PfDyn1 as potential interactors of PfPX2. Globally, these data suggest that PfPX2 is a PIP-binding protein potentially implicated in vesicular trafficking between the Golgi apparatus and the micronemes. Our bioinformatics analyses identified PX2 orthologues across apicomplexans and indeed other alveolates, raising the possibility that this protein plays a role in a broad range of medically, agriculturally, and environmentally relevant organisms.

Keywords Malaria, Protein trafficking, Golgi, PX domain, Phosphoinositides

Although they represent a small percentage of the total lipids found in the eukaryotic intracellular membranes, PIPs serve as crucial regulators of membrane identity and protein trafficking. Their precise spatio-temporal distribution creates a PIP-code, allowing the recruitment of effector proteins and ensuring proper protein transport[1–4]. In *P. falciparum*, PIPs also have compartment-specific localizations and perform essential functions in parasite biology (reviewed in[5] and[6]). The PIP-code is decoded by effector proteins harboring PIP-binding domains, including the Phagocytic oxidase domain of $p40^{phox}$ (PX), which recognizes multiple PIP species with

[1]Department of Microbiology-Infectious Diseases and Immunology, Faculty of Medicine, Université Laval, Québec, QC, Canada. [2]CHU de Québec-Université Laval Research Centre, 2705 Boul. Laurier, Québec, QC G1V 4G2, Canada. [3]Centre de Recherche en Infectiologie de L'Université Laval, Quebec City, QC, Canada. [4]Institute of Animal Biochemistry and Genetics, Centre of Biosciences, Slovak Academy of Sciences, Dubravska Cesta 9, 840 05 Bratislava, Slovakia. [5]Division of Infectious Diseases, Department of Medicine, and Department of Biological Sciences, University of Alberta, 1-124 Clinical Sciences Building, 11350-83 Avenue, Edmonton T6G 2G3, Canada. [6]Centre for Life's Origins and Evolution, Department of Genetics, Evolution and Environment, University College London, Darwin Building, Gower Street, London WC1E 6BT, UK. [7]Institute of Parasitology, Biology Centre, Czech Academy of Sciences, Branišovská 1160/31, 370 05 České Budějovice (Budweis), Czech Republic. ✉email: dave.richard@crchudequebec.ulaval.ca

particular affinity for PI3P[7]. In *P. falciparum*, PI3P localizes to the food vacuole (FV) membrane, the apicoplast, and single membrane vesicles[6,8]. It is implicated in the trafficking pathway of host cell cytosol-containing vesicles to the FV, in the regulation of FV and apicoplast dynamics and stabilization[6,8–12]. Recently, PfPX1, a PX-domain protein, was shown to play an important role in the trafficking pathway of hemoglobin from the host erythrocyte to the FV in *P. falciparum*[11].

These discoveries are particularly significant given the global health burden of malaria, which causes 263 million cases and 597000 deaths in 2023, primarily affecting children under 5 years old[13]. Despite significant progress in combating malaria over the last 20 years, the escalating prevalence of resistance to a wide range of antimalarial drugs, including essential artemisinin-based therapies, underscores the urgent necessity for developing novel therapeutics[14,15].

The formation of specialized secretory organelles such as micronemes, rhoptries, and dense granules is a hallmark of *Plasmodium* merozoites and a prerequisite for host cell invasion. While the mechanisms underlying the biogenesis of these organelles remains incompletely understood, recent studies have provided key insights. A landmark study using expansion microscopy has revealed that organelles such the Golgi, the inner membrane complex (IMC), and rhoptries are assembled around the microtubule organizing center (MTOC), forming a spatially organized network during schizogony[16]. Rhoptry biogenesis follows a sequential pattern beginning with the formation of a nascent rhoptry bulb, followed by the emergence of the characteristic neck-like structure observed in mature merozoites[16–18]. Similarly, micronemes exhibit organizational heterogeneity, forming two distinct populations: An initial subset containing Apical Membrane Antigen-1 (AMA1) followed by a second population containing Erythrocyte Binding Antigen-175 (EBA-175)[16,19]. These sequential biogenesis patterns suggest that cargo loading at Golgi is highly regulated. Among the few molecular players implicated in this process, the Golgi-associated protein PfSortilin has emerged as a potential escort, essential for the trafficking of proteins to the rhoptries, micronemes, and dense granules[20,21]. These findings point to the existence of a tightly regulated sorting of secretory organelle proteins, but the specific mechanisms governing their differential trafficking from the Golgi apparatus remain largely elusive.

To enhance our understanding of the roles of PIPs in *P. falciparum* erythrocytic stage biology. we previously performed a knockout screen of putative PIP-binding proteins[11]. We here present the characterization of Pf3D7_0704400, a PX domain-containing protein for which we could not generate a knockout line, suggesting that it is required for in vitro asexual growth. Since a first PX protein was previously characterized and named PfPX1, we named Pf3D7_0704400 "PfPX2" to follow this nomenclature. Examination of its predicted structure led us to identify canonical and non-canonical PIP-binding motifs in the PfPX2 PX domain. Additionally, a positively charged putative binding pocket was also found. Lipid overlay assay demonstrated the ability of the PfPX2 PX domain to bind multiple PIP species. Immunofluorescence studies localized pools of PfPX2 to the Golgi apparatus and the micronemes during the developing schizonts stage. Finally, proximity labelling identified the heavy chain of clathrin, PfDyn1 and PfSortilin in proximity of PfX2 raising the possibility that they are potential interactors. Collectively, these observations suggest that PfPX2 may play a role in vesicular trafficking between the Golgi apparatus and the micronemes in *P. falciparum*, and with the identification of orthologues in other alveolates, potentially in a much wider span of related organisms as well.

Results and discussion

PfPX2 is a phosphoinositide-binding protein

To gain insight into the putative PIP-binding specificity of the PfPX2 PX domain, we first performed an analysis of its predicted structure using AlphaFold3[22] and ChimeraX[23] for visualization and structural analysis. PfPX2 is a 1010 amino acid protein with a putative PX domain located at its N-terminus (AA: 1–111), followed by four WD40 repeat (WRD) domains and an additional uncharacterized domain of eight parallel ß-sheets (Fig. 1A) The combination of a PX domain with WDRs is uncommon in eukaryotes[24]. In *P. falciparum*, 80 putative WDR containing genes are present, but only PfPX2 possesses this particular architecture[24]. Each WDR contains four anti-parallel ß-sheets that together form a ß-propeller. This ß-propeller provides a stable scaffold for protein–protein interactions. WDR proteins are involved in several cellular processes like signal transduction, vesicular trafficking, cytoskeletal assembly, cell cycle control, chromatin dynamic and gene regulation. Most of the WDR-containing proteins have additional domains with functional activities[25].

Whilst numerous PX domains can bind several types of PIPs, some have a preferential affinity for PI3P[7,26]. According to their PIP-binding preferences, the PX domains can be classified into four groups: 1- those that are not able to bind any PIP; 2- those that can bind PI3P; 3- those that are able to bind other PIPs but not PI3P; and 4- those that bind other PIPs and PI3P[7]. Similarly to other PX domains, the PfPX2 PX domain contains three antiparallel ß-sheets followed by three α-helices (Fig. 1B). We identified a conserved putative PI3P binding domain made up of arginine (R) 38 at the end of the first ß-sheet directly followed by tyrosine (Y) 39, both known to interact with the inositol ring in confirmed PI3P binding proteins, and R77[7,27]. The PPK loop ΨPxxPxK (Ψ = large aliphatic amino acids: V, I, L, or M) described as responsible for the formation of the PI3P binding pocket[7] is present as L**P**NL**PKK** (AA: 57–63) (Fig. 1C). Non-canonical putative PIP-binding motifs consisting of a histidine (H) or Y residue combined with basic residues in the α1-helix adjacent to the PKK loop can facilitate binding to PIPs other than PI3P[7]. In the PfPX2 PX domain, there is a histidine at position 51 within the α1-helix, but no additional surrounding basic residues are present. Finally, electrostatic surface analysis using the Coulombic tool in ChimeraX revealed a positively charged binding pocket formed by the two terminal lysines of the PPK loop (K62 and K63), as well as R77 and R38 and the Y39 (Fig. 1D).

In order to determine the PIP binding capacity of PfPX2, we recombinantly expressed the WT PX domain or a mutated version where the putative PI3P-binding positively charged residues were mutated to alanine (R38A, K63A, R77A) fused to an N-terminal Glutathione-S-transferase (GST) tag and a C-terminal 6xHis tag. An anti-GST Western blot and Coomassie staining on the purified soluble protein revealed a major band at the expected

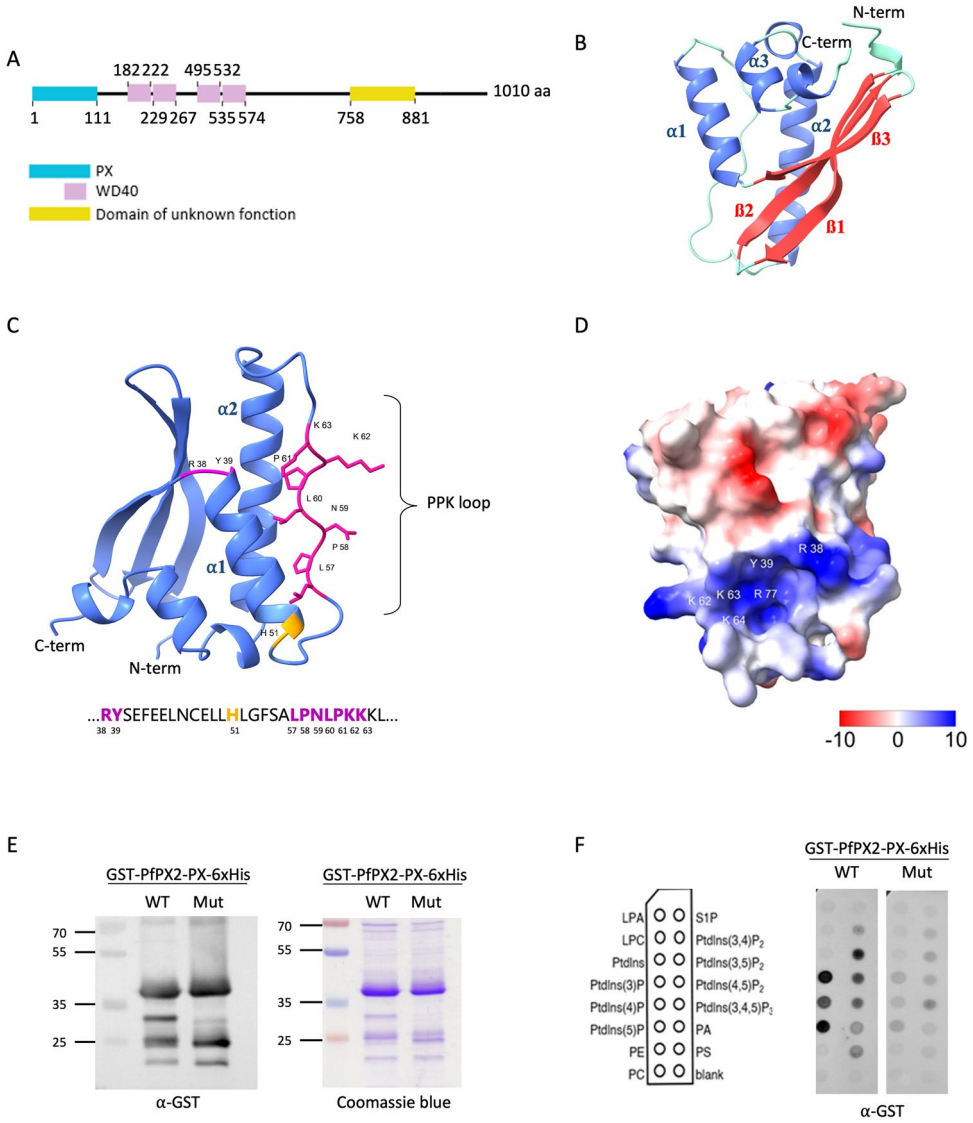

Fig. 1. PfPX2 is a phosphoinositide-binding protein. (**A**) Schematic of PfPX2 with putative predicted domains. (**B**) Structural prediction of the PX domain of PfPX2 showing the three ß-sheets followed by three α-helices. (**C**) Predicted structure of the PfPX2 PX domain showing the canonical PI3P-binding motif, highlighted in pink, and the histidine just before the PPK loop forming the potential non-canonical motif implicated in binding other PIPs, shown in yellow. (**D**) Electrostatic surface view of the PfPX2 PX domain showing the potential positively charged binding pocket with the different amino acids involved. Scale from negatively (red) to positively charged (blue). (**E**) Anti-GST Western blot and Coomassie-stained gel showing the purification of recombinant GST-PfPX2-PX-6xHis WT and a mutant (Mut) where amino acids forming the putative PI3P-binding motif are mutated (R38A, K63A, R77A). (**H**) Lipid blot showing that the GST-PfPX2-PX-6xHis$_{Wt}$ domain binds strongly to PI3P, PI5P and PI(3,5)P2 and to PI4P, PI(4,5)P2 et PI(3,4,5)P3 to a lesser extent. This PIP binding ability is reduced with the mutant.

size of around 37 kDa (Fig. 1E). The purified proteins were then incubated with PIP-strips, nitrocellulose membranes where 15 lipids are grafted. The PfPX2 WT PX domain showed a strong signal for PI3P, PI5P and PI(3,5)P2 and to a lesser extent most of the other species of PIPs (Fig. 1F). Interestingly, PIP-binding was severely reduced in the mutated version, suggesting that R38, K63 and R77A are not restricted solely to PI3P binding. In addition, this also confirmed that the binding pattern observed with the WT domain was not due to the positively charged 6xHis tag. This broad binding specificity despite the absence of a stretch of basic residues usually making up non canonical PIP-binding motifs is intriguing. However, in some proteins such as SNX13, a single additional basic residue in close vicinity to the histidine appears to be sufficient to induce weak but broad binding to several PIPs[7]. In our case, the canonical motif is well conserved, and the combination with this histidine could potentially explain the binding to PIPs other than PI3P observed in the PIP-strip, even without a basic stretch of AA. The strong signal for PI5P is more surprising, as this specificity is rarely reported for PX domains. While certain eukaryotic PX domains have the ability to bind PI5P, these interactions are generally

weak[7,28]. Considering the limited physiological relevance of PIP-strips, further characterization with liposomes containing different PIP species will be required to better delineate the binding specificity of PfPX2.

PfPX2 is expressed in trophozoite and schizont stages

To investigate the role of PfPX2 in *P. falciparum*, 518 bp of the *PfPX2* C-terminal region was fused to a tandem FK506 binding protein domain (2xFKBP) to enable both functional analysis by knock-sideways and identification of proximal protein by dimerization induced BioID (Di-BioID). Additionally, a GFP tag was incorporated for visualization by fluorescence microscopy. This construct was integrated into the parasite genome by single cross-over recombination using the selection-linked integration strategy previously described[29] (Fig. 2A). Genomic

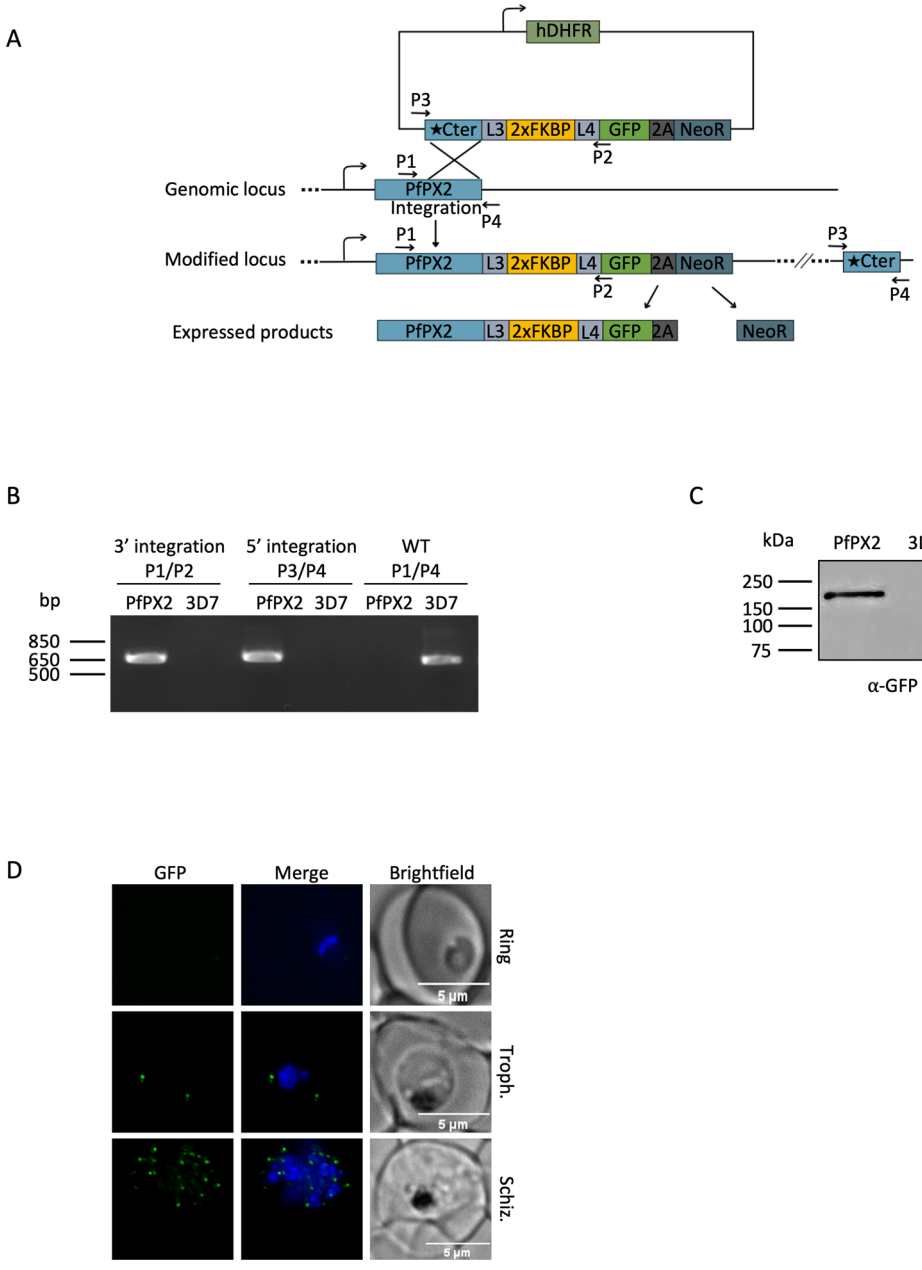

Fig. 2. PfPX2-2xFKBP-GFP line generation and stage-specific expression in the asexual erythrocytic cycle. (**A**) Illustration of the single crossover recombination strategy employed for gene tagging using the SLI system. (**B**) PCR-based validation of tagging vector integration at the *PfPX2* locus performed on parasite genomic DNA from a clonal line. Correct integration was assessed by amplifying junction regions (5′: P1/P2 primers; 3′: P3/P4 primers), while loss of the wild-type allele in PfPX2-2xFKBP-GFP parasites was confirmed using primers P1/P4. (**C**) Anti-GFP western blot on mixed-stage parasite protein extracts showing the proper expression of PfPX2-2xFKBP-GFP at the expected size of around 168 kDa. (**D**) Live microscopy showing that PfPX2-2xFKBP-GFP is expressed in trophozoite and schizont stages. Scale bar represents 5 µm. Blue: DAPI stained nucleus.

integration of the plasmid at the endogenous *PfPX2* locus and the disappearance of the WT allele were confirmed by polymerase chain reaction (PCR) on genomic DNA isolated from a clonal line (Fig. 2B). Immunoblotting of a protein lysate from asynchronous parasites using an anti-GFP antibody detected a band at ~ 168 kD, consistent with the predicted size of the full length tagged protein (Fig. 2C). Live cell imaging revealed no detectable GFP signal in ring stages while one to two foci appeared in trophozoites and became more numerous in schizont stages (Fig. 2D).

PfPX2 localizes to the golgi apparatus and the micronemes

To investigate the subcellular localization of PfPX2 in the parasite, we performed colocalization assays using antibodies against known organelle markers. The colocalization between PfPX2 and the cis-Golgi marker ERD2 was monitored in trophozoites, developing schizonts and late schizonts (incubated with the E64 protease inhibitor to prevent egress[30]). At each stage, we observed some overlap between PfPX2 and ERD2 (Fig. 3A). To quantify the level of colocalization more precisely, we used Pearson's correlation coefficient (PCC) which revealed that the values for trophozoites and developing schizonts were similar (0.68 ± 0.11 and 0.72 ± 0.02 respectively) with no significant difference between them (Fig. 3B). In contrast, the PCC value was slightly but significantly reduced in late schizonts (0.59 ± 0.01) (Fig. 3B). The organelles of the apical complex being generated during the development of schizonts, we next performed colocalization assays with rhoptry (RAP1) and microneme (AMA1) markers at both developing schizont and late schizont stages. In developing schizonts, overlap with PfPX2 can be observed in fluorescence microscopy images for AMA1 but not for RAP1 (Fig. 3C). PCC values showed a marked difference in the colocalization of PfPX2 with these two markers. Specifically, the PCC value for PfPX2 and RAP1 was 0.30 ± 0.13, whereas the PCC with AMA1 was higher, at 0.55 ± 0.01 (Fig. 3D). Including ERD2 in the statistical analysis revealed that PfPX2 colocalized more strongly with the Golgi than with either of the apical markers in developing schizonts (Fig. 3E). For late schizont stages, we no longer observed overlap with AMA1 since it was now secreted on the surface of the merozoites (Fig. 3Civ), as expected[31,32] and as was recently shown in much higher detail by expansion microscopy, with AMA1 below the apical polar ring in developing schizonts before its release on the merozoite in late schizonts[16]. For RAP1, a PCC value of 0.34 ± 0.01 was obtained with no significant difference with the value for developing schizonts (Fig. 3D).

Closer analysis of individual merozoites within individual schizonts showed varying spatial relationships between PfPX2 foci and the different markers. To quantify these patterns, we defined four qualitive categories: (i) no colocalization when green (PfPX2) and red (markers) signals were completely distinct; (ii) close foci when the two signals appeared in close proximity, less than one focus diameter apart, without overlapping; (iii) partial colocalization where the foci shared some overlapping pixels and, finally, (iv) overlap when both signals largely coincided. With the ERD2 marker, 15% of the foci showed a strong overlap, 12% displayed partial colocalization, 37% were in close proximity and 36% showed no colocalization at all (Fig. 3F). Concerning the apical complex markers, a total of 26% of the PfPX2 foci fully overlapped with AMA1 and 48% were found in close proximity. Additionally, 11% of the signal partially overlapped with AMA1, while 15% showed no overlap. In contrast, only 5% of PfPX2 fully overlapped with the RAP1 marker and 6% partially overlapped, whereas 62% were close to RAP1 and 27% showed no overlap. In comparison with ERD2, we observed a larger proportion of PfPX2 foci overlapping with AMA1 in developing schizonts. This contrasts with the higher PCC value for PfPX2-ERD2 compared to PfPX2-AMA1 (0.72 ± 0.02 vs. 0.55 ± 0.01, Fig. 3E). Whilst we cannot explain this discrepancy at this stage we note that this was also recently reported for the *P. falciparum* Tepsin homologue[33]. These observations point to a potential dual localization of PfPX2 at both the micronemes and the Golgi in developing schizonts, suggesting its possible involvement in vesicular transport between these compartments. We cannot currently tell whether PfPX2 is recycled back to the Golgi or exclusively routed toward the micronemes.

Attempts to mislocalize PfPX2 to the nucleus by knock-sideways were unsuccessful

To study the function of PfPX2 during the asexual blood stages, we tried conditional mislocalization by knock-sideways[29]. We first transfected the PfPX2-2xFKBP-GFP line with a mislocalizer construct encoding an FRB-mCherry fusion bearing three nuclear localization signals. Growth assays with rapamycin showed no significant difference in parasite proliferation between the mislocalizer-expressing line and the parental untransfected control (Fig. 4A). Fluorescence microscopy confirmed that the mislocalizer was localized to the DAPI-stained nucleus in the absence of rapamycin (Fig. 4Bi). However, visual inspection revealed that the addition of rapamycin did not result in substantial translocation of PfPX2-2xFKBP-GFP to the nucleus (Fig. 4Bii). PCC analysis revealed only a modest increase in overlap between the Dapi-stained nucleus and GFP, as well as between the mCherry-tagged mislocalizer and GFP, but significantly decreased the overlap between Dapi and mCherry, suggesting relocalization of the mislocalizer to the cytosol (Fig. 4C) as sometimes reported[33,34]. This result indicates that the mislocalizer itself was mislocalized, rather than PfPX2 being efficiently targeted to the nucleus, preventing us from determining whether PfPX2 was required for parasite survival. Our previous unsuccessful attempts to knock out the *PfPX2* gene by SLI[35] and its low mutagenesis index in a genome-wide piggyback screen in *P. falciparum*[36] point to a potential essentiality of the gene. Interestingly, in a recent genome-wide piggyback screen in *P. knowlesi*, insertions were only found at the extreme C-terminus of the *PkPX2* gene[37]. Optimization strategies such as using an alternative mislocalizer (e.g., plasma membrane instead of nucleus), increasing FKBP copy number[34] or switching to other conditional systems like the glmS ribozyme[38] or the TetR-DOZI[39], may help clarify its function.

Identifications of PfPX2 proximal proteins by proximity biotinylation

To uncover potential interaction partners of PfPX2, we performed a Di-BioID experiment, a proximity-labeling technique that captures proteins located near a protein of interest in live parasites[29]. We used the PfPX2-2xFKBP-GFP strain and introduced a construct expressing a promiscuous biotin ligase (BirA), fused to the FKBP12-

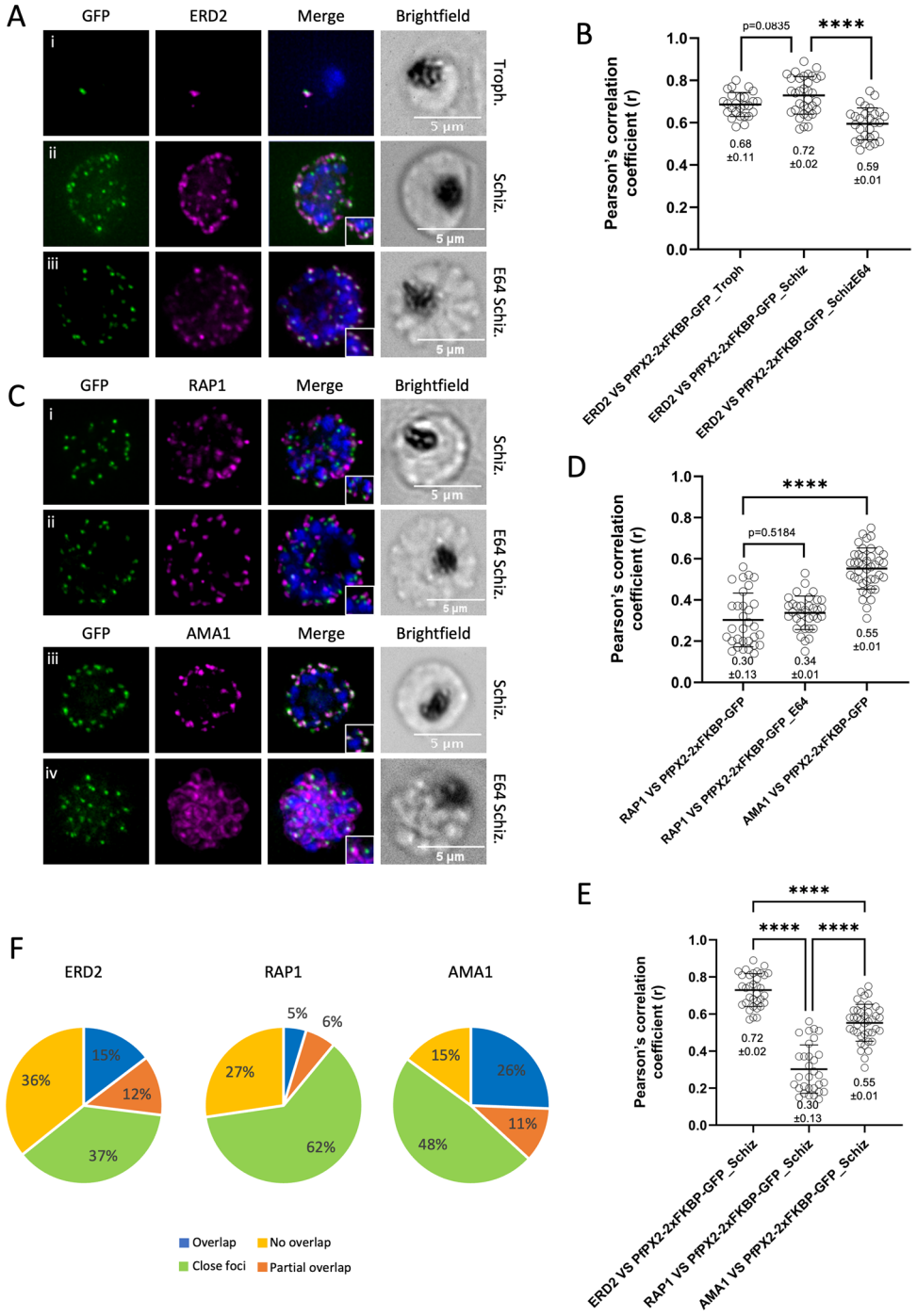

rapamycin binding protein (FRB) domain, which can dimerize with FKBP in the presence of rapamycin, and an mCherry tag. The addition of rapamycin to the culture medium triggers the dimerization between FKBP and FRB, bringing BirA into the immediate vicinity of PfPX2. This setup enables the biotinylation of neighboring proteins, providing a snapshot of its molecular environment[10]. The labeled proteins are then pulled down with streptavidin beads and identified by mass spectrometry (Fig. 5A). To verify if rapamycin led to the dimerization of FRB-BirA-mCherry with PfPX2-FKBP-GFP, live microscopy was performed. In the absence of rapamycin, FRB-BirA-mCherry was diffused throughout the cytoplasm however the addition of rapamycin led to a strong overlap between both signals (Fig. 5B). Streptavidin-Alexa 594 was next used to confirm that protein biotinylation had occurred at the PfPX2 foci upon addition of rapamycin (Fig. 5C).

After a 24 h incubation with rapamycin, cells were lysed and biotinylated proteins were pulled down using streptavidin-beads for proteomics analysis. Three biological replicates were performed, each yielding more than 300 identified proteins (PX2_Dataset-1). Stringent filtering was applied to refine the results: Only proteins with a normalized intensity Rapa + /Rapa- ratio ≥ 1.5 in each replicate were first selected. Of the proteins, only those with at least two unique peptides in the Rapa + sample in at least two out of three replicates were retained, resulting in a final list of 14 proteins (Fig. 5D). PfPX2 itself emerged as the most enriched protein across all the three replicates (with a log2 ratio > 11 in all replicates) consistent with the successful recruitment of FRB-BirA

◀**Fig. 3**. Subcellular localization of PfPX2. (**A**) Immunofluorescence assays to determine the overlap between PfPX2-2xFKBP-GFP and the cis-Golgi marker ERD2 in trophozoites (Ai), developing schizonts (Aii) and late schizonts treated with E64 (Aiii). (**B**) Pearson's correlation analysis reveals that there is no difference in the overlap levels between PfPX2-2xFKBP-GFP and ERD2 in trophozoites and developing schizonts (p value = 0.0835). However, co-localization significantly decreases in late schizonts treated with E64. PfPX2-2xFKBP-GFP vs ERD2, Trophs: n = 26; Developing schizonts: n = 34; E64 schizonts: n = 28. (**C**) Immunofluorescence assays showing that (Ci) PfPX2 does not colocalize with the RAP1 rhoptry marker in either developing schizonts or in (Cii) late schizonts treated with E64. However, there is an overlap between PfPX2 and the microneme marker AMA1 in developing schizonts (Ciii), but not in late schizonts treated with E64 (Civ). (**D**) Pearson's correlation analysis demonstrates that there is no significant difference (p value = 0.5184) in the levels of colocalization between PfPX2-2xFKBP-GFP and RAP1 in developing schizonts and late schizonts but shows a significant difference in colocalization between PfPX2 and AMA1 in developing schizonts. PfPX2-2xFKBP-GFP versus RAP1: Developing schizonts: n = 31; E64 schizonts: n = 34. PfPX2-2xFKBP-GFP versus AMA1: Developing schizonts: n = 41. (**E**) Pearson's correlation analysis demonstrates there is higher overlap between PfPX2-2xFKBP-GFP and ERD2 then with either RAP1 or AMA1 in developing schizonts. PfPX2-2xFKBP-GFP versus ERD2: n = 34; PfPX2-2xFKBP-GFP versus RAP1: n = 31; PfPX2-2xFKBP-GFP versus AMA1: n = 41. (**F**) Quantification of the foci distribution in individual merozoites in developing schizonts. Overlap in blue; partial overlap in orange; close foci in green and no overlap in yellow. PfPX2-2xFKBP-GFP versus ERD2: n = 44; PfPX2-2xFKBP-GFP versus RAP1: n = 31; PfPX2-2xFKBP-GFP versus AMA1: n = 32. Raw data available in supplementary file named Colocalization_counts_PfPX2. Scale bar represents 5 µm. Blue: DAPI stained nucleus. Troph: trophozoites. Schiz: developing schizonts. For all PCC analyses, data were pooled from 3 biological replicates. Values represent the mean ± standard error. Statistical analysis was performed using an unpaired t-test student: ****: $p < 0.0001$.

to PfPX2-2xFKBP-GFP. The identification of PfFKBP35 is likely due to the 2xFKBP tag. A number of interesting proteins were identified: PfSortilin had a log2 ratio > 6. Sortilin is a transmembrane protein known for its role as an escort protein in eukaryotic cells and is a key component of the vesicular trafficking pathway, cycling between the Golgi and the endosomes[40]. In both *P. falciparum* and *T. gondii,* Sortilin has been shown to be essential and mediate transport of proteins destined for the micronemes, rhoptries and dense granules as well as potentially contributing to the biogenesis of the inner membrane complex (IMC) in *P. falciparum*[20,21,41]. The potential interaction between PfSortilin and PfPX2 might suggest an involvement of PfPX2 in vesicular trafficking from the Golgi to the apical complex and the IMC.

The identification of the heavy chain of clathrin as a putative interactor of PfPX2 is consistent with a previous study of the putative interactome of PfClathrin that also identified PfPX2[42], supporting that both proteins are potentially interacting, despite PfPX2 having no canonical clathrin-binding motif[43]. In mammalian cells, clathrin is localized at the trans-Golgi network and plasma membrane where it plays keys roles in processes such as clathrin-mediated endocytosis, protein sorting and trafficking and the regulation of membrane composition[44]. In *T. gondii*, clathrin is involved in vesicular transport to the IMC, plasma membrane, micronemes, and rhoptries, without evidence for its implication in endocytic processes[45]. Though it was initially thought that clathrin was not involved in hemoglobin endocytosis in *P. falciparum*[10,42], a preprint on bioRxiv has shown that conditionally knocking down the clathrin heavy chain leads to elongated cytostomes and impaired hemoglobin digestion[46]. Although there is currently no functional evidence for the existence of canonical endosomes in *P. falciparum*, cellular compartments labelled with endocytic markers such as Rab5B, RbsnL, Rab7 and retromer components have been identified[47,48].

The dynamin-like protein PfDyn1 is of particular interest because dynamins have established roles in vesicular fission during clathrin-mediated endocytosis in mammalian cells[49] as well as in microneme and rhoptry biogenesis and endocytosis at the plasma membrane in *T. gondii*[50,51]. *P. falciparum* encodes three dynamin-related proteins and PfDyn1 was suggested to have a role in hemoglobin endocytosis[52,53].

A Vps13-domain containing protein was also identified and homologues of these act as tethers at membrane contact sites (MCS) in eukaryotic cells[54]. Some proteins with PX domains, such as Sorting Nexins, are known to be implicated at MCS so perhaps PfPX2 might also play a role at these peculiar cellular structures. A GRIP domain containing protein was also present and recent work has shown that like PfPX2, it also localizes to the Golgi apparatus. Its function is currently unknown[55], but the protein is likely essential for in vitro asexual growth[34].

The rest of the identified proteins are potentially contaminants since these are often found in BioID and immunoprecipitation experiments (cytosolic enzymes: phosphoglycerate kinase, casein kinase 1; protein involved with DNA/RNA: BSD-domain protein, eIF2gamma, nuclear movement protein, BRR2 helicase; a V-type proton ATPase catalytic subunit…).

In conclusion, the identification of PfSortilin, PfDyn1, and the clathrin heavy chain as proteins proximal to PfPX2 could suggest a potential role of the latter in vesicular trafficking.

Orthologues of PfPX2 are present in diverse alveolates

In order to better understand the taxonomic distribution of PfPX2, and in turn ask whether the experimental data obtained may be potentially applicable to other related microbial eukaryotes, homology searching with BLAST and HMMer searches was conducted in taxa from the Stramenopiles, Alveolates and Rhizarians (SAR) eukaryotic supergroup with more emphasis on Apicomplexan (PX2_Dataset-2). Homology searching using the full length of PfPX2 retrieved proteins with only PX domains from stramenopiles, rhizarians, some ciliates,

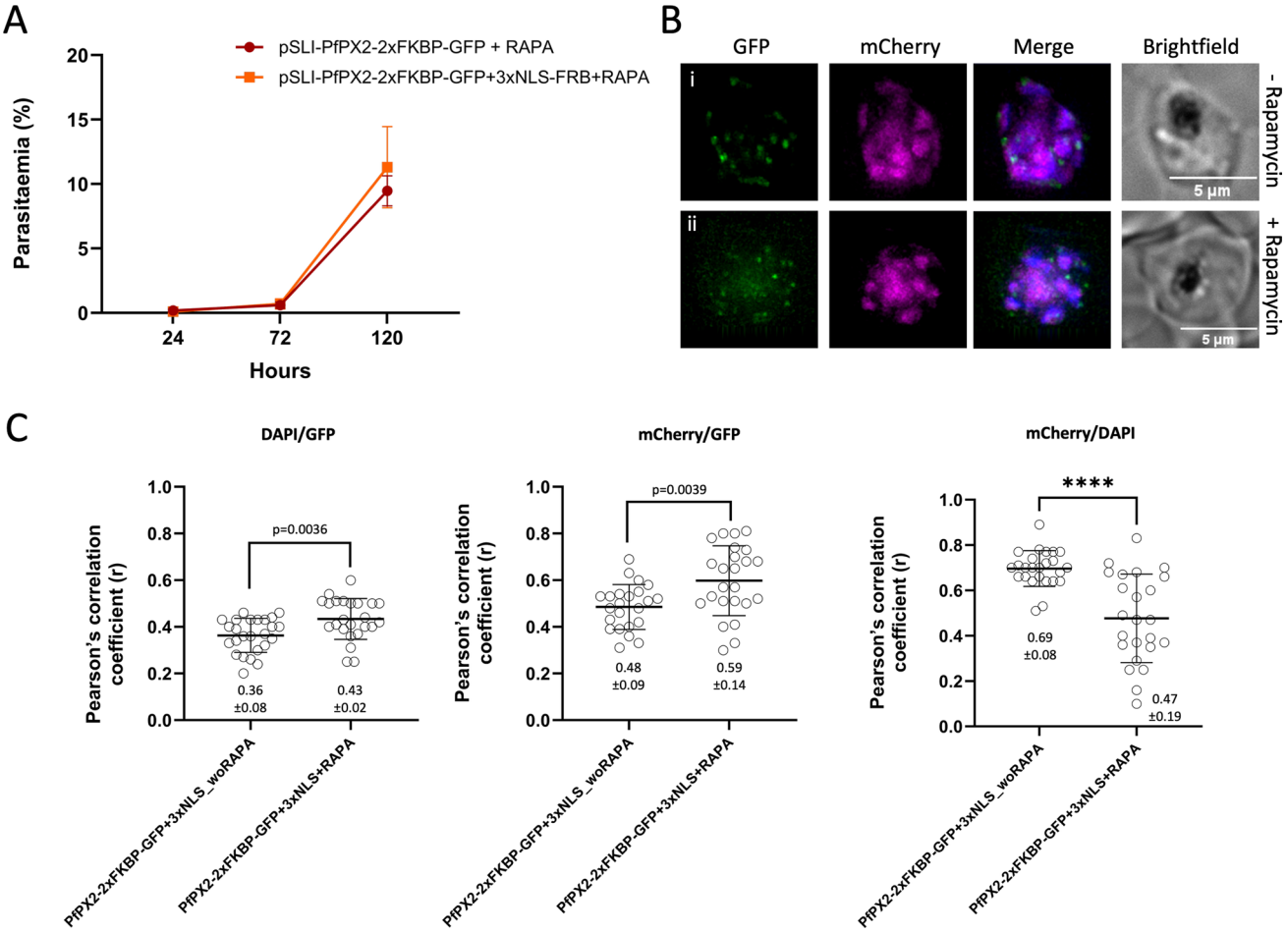

Fig. 4. Knock-sideways attempt. (**A**) Growth curve showing no difference in parasitemia between the PfPX2-2xFKBP-GFP strain expressing the 3xNLS-FRB-mCherry mislocalizer (orange) and the strain without (red), in the presence of rapamycin (RAPA). Mean ± SEM of four replicates are shown. 3xNLS-FRB = 3xNLS-FRB-mCherry. (**B**) Live cell microscopy showing limited translocation of the PfPX2-2xFKBP-GFP to the nucleus upon addition of rapamycin. Scale bar represents 5 µm. Blue: DAPI stained nucleus. (**C**) Pearson's correlation analysis reveals that rapamycin addition causes some of the mislocalizer to translocate from the nucleus to the cytosol. 3xNLS: 3xNLS-FRB-mCherry. Data were pooled from 3 biological replicates. Values represent the mean ± standard error. PfPX2-2xFKBP-GFP + 3xNLS-FRB-mCherry without rapamycin: n = 25; with rapamycin: n = 24. *P* values were calculated using an unpaired t-test. ****: $p < 0.0001$.

dinoflagellates and apicomplexans. To remove false positives, additional searches using the protein but excluding the PX domain were performed. Only hits with both a PX domain and WD repeats were considered positive hits. However, negative hits are also given in the document PX2_Dataset-2.

Based on the given criteria, PfPX2 was found to be well conserved in all selected apicomplexans (Fig. 6), except in *Cryptosporidium* spp. and *Eimeria tenella*. Consistent with the proposed Golgi association inferred from our work, the *T. gondii* orthologue (TGME48_228400, referred to TgPX4 in[56]) appears to co-localize with a Golgi marker GRASP[56]. Outside Apicomplexa, PfPX2 was also present in Dinoflagellata (except *Durudinium* sp. and *Procentrum minimum*), Ciliophora, and Colpodellida (Fig. 6). Among ciliates, true orthologs were identified in *Tetrahymena thermophila, Paramecium caudatum, P. tetraurelia, Euplotes octocarinatus, Stylonychia lemnae.* In *Blepharisma japonicum* and *Stentor coeruleus*, ciliate sequences were either partial or with only a PX domain. Absence of putative orthologs in stramenopiles and rhizarians indicates the conservation of PfPX2 within alveolates, but a potential emergence point after their divergence from the other SAR groups.

The conserved domain organization of PfPX2, with multiple WD40 repeats C-terminal to the PX domain, is retained across diverse alveolate taxa, and sets the proteins apart from the previously characterized *Plasmodium*-specific protein PfPX1[35], which possesses potential transmembrane domains. Notably, the canonical RY and PPK PIP binding motifs (ΨPxxPxK) are highly conserved and present in a homologous position in nearly all of the alveolate orthologues that we identified (Fig. S1). This domain organization and motif conservation lends further weight to a hypothesis of conserved function (PIP binding and more speculatively functional homology based on the other experimental data as well) for the protein in these other organisms as well.

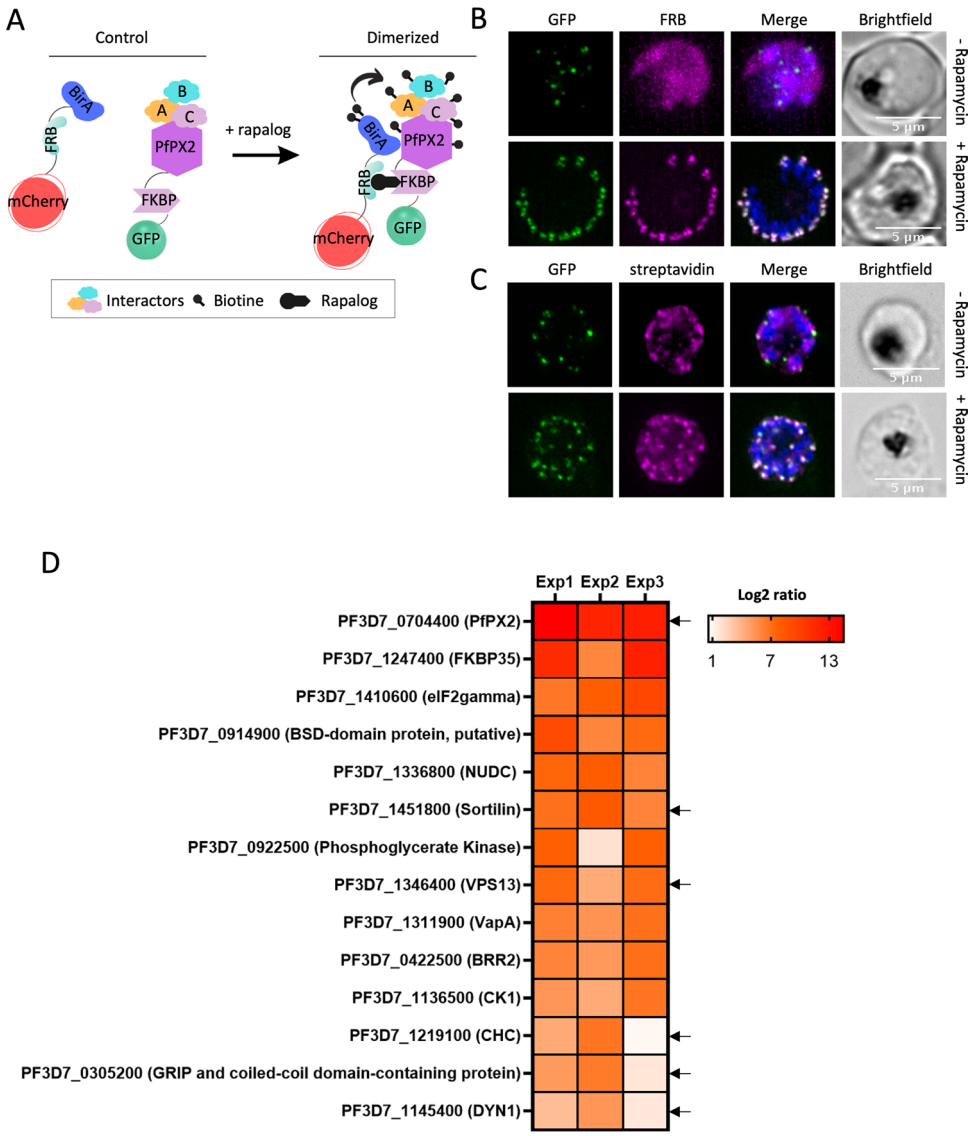

Fig. 5. Identification of PfPX2 proximal proteins by Di-BioID. (**A**) Illustration of the Di-BioID principle. (**B**) Live microscopy demonstrating that incubation of the PfPX2-2xFKBP-GFP + FRB-BirA-mCherry parasite line with 250 nM rapamycin for 24 h results in the translocation of the mCherry signal to PfPX2-2xFKBP-GFP foci. Scale bar = 5 µm. Blue: DAPI-stained nuclei. (**C**) Immunofluorescence analysis with anti-streptavidin confirmed successful biotinylation at the PfPX2-2xFKBP-GFP foci (**D**) Heat map showing proteins with ≥ 1.5-fold enrichment across three biological replicates. Data expressed as log2. Arrows indicate PfPX2, PfSortilin, VPS13, the clathrin heavy chain, GRIP and coiled-coil domain-containing protein and PfDyn1.

Conclusion

The potential interaction of PfPX2 with PfDyn1, PfSortilin and clathrin and its localization to the Golgi and micronemes suggests a possible role for PfPX2 in vesicular trafficking to the apical complex and perhaps more specifically to the micronemes though functional analysis using other conditional systems will be required to test this hypothesis. Notably, Dyn1 and Sortilin proteins have been implicated in the biogenesis of apical organelles in *T. gondii*[41,50] as well as PfSortilin in *P. falciparum*[21]. In mammalian cells, dynamins, Sortilin and clathrins are known to play crucial roles in endocytic pathways[40,44,52,53,57]. As stated above, although no classical endosomes have been functionally characterized in *P. falciparum*, some intracellular compartments have been shown to interact with established endosomal markers such as Rab7 and the retromer components, suggesting the presence of endosome-like compartment (ELC)[47]. Moreover, these ELC have been previously hypothesized to participate in the trafficking of apical complex proteins[21,47]. The ability of PfPX2 to bind PIPs might suggest that these lipids are involved in vesicular trafficking to the apical complex in *P. falciparum*.

Fig. 6. PfPX2 orthologues are conserved across Alveolates. Schematic of PfPX2 and its orthologues showing the position of PX domain followed by WD40 repeats containing domain. Conserved domain structures are shown based on InterProScan[65]. Dendrogram shows the relationship between taxa. Accession number and length of PfPX2 orthologues in all selected taxa are mentioned. Aa, amino acids. Brown box: Conserved PX domain. Purple: WD40 repeats like domain. Dark purple: WD 40 repeats.

Materials and methods

Ethics statement

Study approved by the Canadian Blood Services (CBS) research ethics board, project number 2015.001 and by the CHU de Québec IRB, project number 2015–2230, B14-12-2230, SIRUL 104,595. Informed consent was obtained from all Participants. Participants were informed about the study before providing consent. All experiments were performed in accordance with relevant guidelines and regulations.

Protein structure analysis

The PfPX2 structure prediction was made using AlphaFold3[22] and UCSF ChimeraX. The electrostatic surface analysis was performed using the « color surface by electrostatic potential » tool from USCF ChimeraX. The electrostatic potential was performed using the Coulombic Surface Coloring method based on Coulomb's law: $\Phi = \Sigma[qi/\epsilon di]$, where Φ represents the potential, q corresponds to the atomic partial charges, d indicates the distances from the atoms, and ϵ is the dielectric constant. The resulting electrostatic potential was mapped onto the molecular surface using a color gradient going from red which signifies a negative potential, through white which denotes a neutral potential to blue indicating a positive potential.

Production and purification of the recombinant PfPX2 PX domain

The PX domain of PfPX2 (amino acids 4–107) was amplified on 3D7 WT mixed stages cDNA using the primers 5′BamH1-PfPX2domain (ATAGGATCCATGGACTTAGAAAAGTTTGAC) and 3′Xho1-PfPX2domain (ATACTCGAGGGTTTTAACGATATCTATAGATAAATTTATTTTAT). The PX domain mutant sequence (R38A, K63A, R77A) was custom synthetized by Integrate DNA technologies (IDT, Coralville, IA, USA). BamH1 and Xho1 restrictions sites were introduced by PCR using the same primers as above. Both the wild-type and mutant PfPX2 domain were cloned in pGEX-6P3 (GE Healthcare) giving the plasmids pGEX-PfPX2dom_wt and mutant. The pGEX-PfPX2dom_wt and mutant plasmids were then modified by adding a 6×His tag to the C-terminus. The PX2 domains were amplified by PCR using the primers PX2 Fwd (5′-ATAGGATCCATGGACTTAGAAAAGTTTGACATTC-3′) and PX2 Rev (5′-GTATGCGGCCGCTCAGTGGTGGTGGTGGTGGTGCGACCCCCCCGACCCCCCATTTATTTTATCATAAAATAAAAGGAAATT-3′). This PCR introduced a *BamH*I restriction site at the N-terminus of the PX2 domains and a six-amino-acid linker (GGSGGS) at the C-terminus, followed by a 6×His tag, a stop codon, and a *Not*I restriction site. The resulting PCR products replaced the PX domain in the pGEX-PfPX2dom_wt and mutant plasmids via the *BamH*I and *Not*I restriction sites, creating plasmids pGEX-PfPX2dom_wt-6xHis and pGEX-PfPX2dom_mut-6xHis, respectively. All constructs were verified by sequencing. The pGEX-PfPX2dom_wt-6×His and pGEX-PfPX2dom_mut-6×His plasmids were transformed into *Arctic Express* (DE3) *E. coli* (Agilent) for protein expression. Ten mL of overnight cultures containing 100 µg/mL ampicillin and 20 µg/mL gentamicin were used to inoculate 500 mL of TB medium supplemented with the same antibiotics. The cells were grown for 4 h at 30 °C with constant shaking. Protein expression was then induced with IPTG (final concentration: 400 µM), and the cultures were incubated overnight at 10 °C. After incubation, the cells were centrifuged, the pellet was washed twice with ice-cold water, and stored at − 80 °C.

The bacterial pellet was thawed on ice and resuspended in 15 mL of lysis buffer (25 mM Tris–HCl, pH 7.4; 300 mM KCl; 10% glycerol; 0.5% Tween-20; 10 mM imidazole, pH 7.4), supplemented with one tablet of protease inhibitors (cOmplete™ ULTRA Tablets, EDTA-free; cat. no. 05892953001, Roche) per 10 g of wet bacterial cell weight. Cells were lysed using a French Pressure Cell Press (Sim Aminco, SLM Instruments, Inc.) at 1250 PSI. The lysate was subsequently sonicated (Soniprep 150, MSE Supplies) for 30 s at 15 µm amplitude, then centrifuged at 25,000×*g* for 20 min at 4 °C using an Optima L-100XP ultracentrifuge (Beckman Coulter).

The cleared lysate was loaded onto a gravity column containing Ni–NTA resin (cat. no. 786–1547, G-Biosciences) pre-equilibrated with lysis buffer. The column was washed three times with wash buffer (25 mM Tris–HCl, pH 7.4; 300 mM KCl; 10% glycerol; 0.1% Tween-20; 40 mM imidazole, pH 7.4). PX2 domains were eluted with elution buffer containing increasing concentrations of imidazole (100–300 mM) in the same base buffer (25 mM Tris–HCl, pH 7.4; 300 mM KCl; 10% glycerol; 0.1% Tween-20). Eluted fractions were analyzed by SDS-PAGE to assess protein yield and purity. Fractions with the highest purity and concentration were pooled and desalted using a PD-10 column (GE Healthcare) to remove imidazole. The final protein was eluted in buffer containing 25 mM Tris–HCl, pH 7.4; 300 mM KCl; and 10% glycerol. Protein concentration was determined by using a BSA standard curve by SDS-PAGE. The purified PX2 domains were aliquoted and stored at − 20 °C.

Protein–lipid overlay assay

Echelon P6001 strips (Echelon Biosciences), containing immobilized lipids, were first incubated in 3% BSA (fatty acid-free; cat. no. A7030, Sigma-Aldrich) in TBS-T (50 mM Tris–HCl, pH 7.5; 150 mM NaCl; 0.1% [v/v] Tween-20) for 1 h at room temperature to block non-specific interactions. Following blocking, the membranes were washed three times for 10 min each with washing buffer (50 mM Tris–HCl, pH 7.5; 150 mM NaCl; 0.05% [v/v] Tween-20). The membranes were then incubated overnight at 4 °C with recombinant PX2 domains (final concentration: 1 µg/mL).

The next day, the membranes were washed three times with washing buffer and incubated with an anti-GST primary antibody for 2 h at room temperature. After washing three times, the membrane was incubated with secondary antibodies (an anti-mouse IgG HRP conjugate (cat. no. 12349, Sigma; 1:40,000 dilution) for 1 h at room temperature. A final wash (three times with washing buffer) was performed before detection. PX2 domains were visualized by chemiluminescence using the SuperSignal™ West Pico PLUS Chemiluminescent Substrate (cat. no. 34580, Thermo Fisher) and the Imager Chemi Premium (VWR).

Parasite culture

P. falciparum 3D7 asexual stage parasites provided by David Walliker, Edinburgh University were cultivated under standard conditions in RPMI-HEPES medium at 4% hematocrit (human erythrocytes of O + group) and 0.5% (w/v) Albumax™ (Invitrogen) and maintained at 37 °C in a gas mixture of 5.0% oxygen, 5.0% carbon dioxide and 90% nitrogen[58].

Vector constructions and transfection

PfPX2 was endogenously tagged with 2xFKBP-GFP with the selection-linked integration strategy[29]. Approximately 500 bp of the N-terminus of PfPX2 was amplified using the following primers: 5′Not1-Pf3D7-0,704,400 (ATAGCGGCCGCGTATGATATATAATAATGCTATTC) and 3′AvrII-stopless-Pf3D7-0,704,400 (ATACCTAGGTCTAAATGCCGATATTAAATC). This 500 pb fragment of PfX2 was then digested with NotI and AvrII and cloned in frame with 2xFKBP-GFP into the pSLI-2xFKBP-GFP vector, which had already been digested with the same restriction enzyme. Transfection and selection were carried out as previously described[3]. Briefly, *P. falciparum* 3D7 parasites were transfected with 100 µg of the pSLI-PfPX2-2xFKBP-GFP plasmid. A primary positive selection was performed with 5 nM WR99210 (WR, Jacobus Pharmaceuticals). To ensure the selection of integrants, the parasites underwent a second round of selection using 400 mg/mL neomycin (NEO). WR was reintroduced into the culture media after the parasite reemerged, which took approximately 10 days. Proper integration of the plasmid was verified by PCR using the following primer pairs: for the integration in 5′, a GOI-specific forward primer 1 (GTATAATATATAATAATGCTAGCCAAG) along with primer 2: FKBP-sandwich-rev (CAGAGCAGCTCTAGCAGC). For the 3′ integration event, primer 3: M13_rev (CAGGAAACAGCTATGAC) and a GOI-specific reverse primer 4: (CATATATTCGTGGATGCTCTTG).

Western blotting

Saponin-extracted parasites from a mixed stages culture of the PfPX2-2xFKBP-GFP line were harvested, and the pellet was subsequently solubilized in SDS protein sample buffer. Proteins were separated using a 7% (wt/vol) SDS–polyacrylamide gel under reducing conditions and transferred to a polyvinylidene difluoride (PVDF) membrane (Millipore). Blocking was performed with 4% (wt/vol) milk in Tris-buffered saline with Tween 20 (TBS-T) for 30 min at RT. Followed by a first incubation with a mouse monoclonal anti-GFP (clone JL-8; Roche) (diluted 1:1000) during 1 h at RT and with a mouse horseradish peroxidase (HRP)-coupled secondary antibodies (Sigma) (diluted 1:10 000) 30 min at RT. Immunoblots were developed using ECL (Bio-Rad).

Colocalization assays

All the fluorescence images of parasites were acquired using a GE Applied Precision Deltavision Elite microscope equipped with 100 × 1.4NA objective and with a sCMOS camera. Images were subsequently deconvolved using the SoftWorx software. Prior to imaging experiments, chromatic calibration of the microscope was performed to ensure accurate color representation. For immunofluorescence assays, parasites were fixed using 4% paraformaldehyde (ProSciTech)[5] on pre-treated coverslip with 0.01% v/v poly-L-lysine. Parasites were then permeabilized with 0.1% Triton X-100 (Sigma-Aldrich). A blocking step of 1 h was done with 3% bovine serum albumin (Sigma Aldrich) followed by a 1 h incubation with primary antibodies: Rabbit polyclonal anti-PfERD2 (1:2000)[59], mouse monoclonal anti-RAP1 (1:2000)[60], mouse monoclonal anti-AMA1 (clone 1F9; 1:1000)[61], anti-HA (1:1000) and anti-streptavidin-Alexa Fluor 660 conjugate (1:500). Finally, unless for parasites incubated with the conjugated anti-Streptevidin Alexa Fluor 660, parasites were incubated with a secondary antibody either Fluor-594 anti-rabbit or anti-mouse diluted at 1:1000 (Cedarlane). Parasites were mounted in Vectashield (Vecta Laboratories) containing 0.1 mg/ml 4′, 6–diamidino-2-phenylindole (DAPI, Invitrogen). For live-cell imaging, PfPX2-2xFKBP-GFP parasites and the co-transfected lines with the FRB-BirA-mCherry plasmid and 1xNLS-FRB-mCherry were harvested in trophozoite and/or schizont-stages and incubated with DAPI 10 min prior to visualizing them. Images shown represent a single optical slice from a deconvolved z-stack.

Knocksideways attempts

PfPX2-2xFKBP-GFP + mislocalizer parasites were tightly synchronized in ring stage and plated at initial parasitemia of 2% and cultured in the presence of 250 nM rapamycin. Once they reached the schizont stage, the cells were harvested, stained with DAPI (100 ng/µL, Invitrogen) to be immediately imaged by live microscopy. To assess growth dynamics, PfPX2-2xFKBP-GFP cultures (with and without mislocalizer) were initiated at 0.1% parasitemia and maintained under 250 nM rapamycin exposure. Parasites samples were collected at 24, 72, and 120 h intervals, and stained with SYBR Gold (Invitrogen-Molecular Probe), followed by fixation with 1% paraformaldehyde for 1 h. Flow cytometry analysis was performed using a BD FACSCantoII system running FACSDiva software to quantify parasitemia levels. Data processing and analysis were conducted through FlowJo software. Uninfected red blood cells were used as control to determine the fluorescein isothiocyanate signal threshold.

Preparation of samples for Di-BioID

Late ring-stage parasites from PfPX2-2xFKBP-GFP + FRB-BirA-mCherry line were incubated with 50 µM of biotin (Sigma-Aldrich) and, depending on the condition, with or without 250 nM of rapamycin (RAPA—R0395, Sigma) for 20–24 h. Live-cell microscopy on schizont-stage parasites confirmed the proper dimerization between PfPX2 protein and BirA. Aditionnally, an IFA using streptavidin-conjugated AlexaFluor660 (Invitrogen) was performed to verify biotinylation. The DiQBioID experiments were then conducted as previously described[9]. Parasites were harvested and washed twice in PBS before being lysed by saponin and then frozen at − 80 °C. The pellets were thawed and resuspended in 2 ml of cold lysis buffer (50 mM Tris–HCl pH 7.5, 500 nM NaCl, 1% Triton X-100 (Sigma-Aldrich), 1 mM dithiothreitol (DTT, Sigma-Aldrich), 1 mM phenylmethylsulfonyl fluoride

(PMSF, Sigma-Aldrich) and a CØmplete EDTA-free protease inhibitor cocktail tablet (Roche)). The pellets underwent two freeze–thaw cycles followed by cell disruption using 3 rounds of sonication (Fisher Scientific, model 100) for 10 s each with 30 s breaks. After centrifugation at 16000×g, the supernatants were incubated with streptavidin agarose beads (Invitrogen) at 4 °C O/N to enrich for biotinylated proteins. Finally, the beads were washed twice with lysis buffer, once in dH2O, twice in Tris–HCL (pH 7.5), and five times in 50 mM ammonium bicarbonate (Sigma-Aldrich) before being sent for mass spectrometry analysis.

Sample preparation and data acquisition for mass spectrometry analysis

Protein digestion

Protein digestion and mass spectrometry experiments were performed by the Proteomics platform of the CHU de Quebec Research Center, Quebec, Canada. On beads protein digestion was carried out using 0.1 µg of modified porcine trypsin (sequencing grade, Promega, Madison, WI) in 50 mM ammonium bicarbonate for 5 h at 37 °C. Digestion was stopped with 5% formic acid (FA) and peptides were eluted from the beads with 60% acetonitrile (ACN) 0.1% FA. Tryptic peptides were desalted on Stage tips (Empore C18, 3 M Company), vacuum dried then resuspended in LC loading solvent (2% ACN, 0.05% trifluoroacetic acid (TFA)).

Mass spectrometry

Half of each sample was analysed by nanoLC/MSMS using a Dionex UltiMate 3000 nanoRSLC chromatography system (Thermo Fisher Scientific) connected to an Orbitrap Fusion mass spectrometer (Thermo Fisher Scientific, San Jose, CA, USA) equipped with a nanoelectrospray ion source. Peptides were trapped at 20 µl/min in loading solvent (2% ACN, 0.05% TFA) on a 5 mm × 300 µm C18 pepmap cartridge (Thermo Fisher Scientific) for 5 min. Then, the pre-column was switched online with a 50 cm x 75 µm internal diameter separation column (Pepmap Acclaim column, ThermoFisher) and the peptides were eluted with a linear gradient from 5–40% solvent B (A: 0.1% FA, B: 80% ACN, 0.1% FA) in 30 min, at 300 nL/min (60 min total run time). Mass spectra were acquired using a data dependent acquisition mode using Thermo XCalibur software version 4.1.50. Full scan mass spectra (350 to 1800 m/z) were acquired in the orbitrap using an Automatic Gain Control (AGC) target of 4e5, a maximum injection time of 50 ms and a resolution of 120 000. Internal calibration using lock mass on the m/z 445.12003 siloxane ion was used. Each MS scan was followed by acquisition of fragmentation MSMS spectra of the most intense ions for a total cycle time of 3 s (top speed mode). The selected ions were isolated using the quadrupole analyzer with 1.6 m/z windows and fragmented by Higher energy Collision-induced Dissociation (HCD) with 35% of collision energy. The resulting fragments were detected by the linear ion trap in rapid scan rate with an AGC target of 1e4 and a maximum injection time of 50 ms. Dynamic exclusion of previously fragmented peptides was set for a period of 30 s and a tolerance of 10 ppm.

Database searching

MGF peak list files were created using Proteome Discoverer 2.3 software (Thermo). MGF files were then analyzed using Mascot (Matrix Science, London, UK; version 2.8.0). Mascot was set up to search a contaminant database and Uniprot *Plasmodium falciparum* 3D7 (5538 entries, reference proteome UP000001450) database assuming the digestion enzyme trypsin. Mascot was searched with a fragment ion mass tolerance of 0.60 Da and a parent ion tolerance of 10.0 PPM. Carbamidomethyl of cysteine was specified in Mascot as a fixed modification. Deamidation of asparagine and glutamine and oxidation of methionine were specified in Mascot as variable modifications. 2 missed cleavages were allowed.

Protein identification and data analysis

Mass spectra were searched against the Uniprot *Plasmodium falciparum* 3D7 database (5538 entries, reference proteome UP000001450, downloaded 2021.04) using the search engine Andromeda integrated into the MaxQuant software (version 2.0.2.0) assuming the digestion enzyme trypsin. Protein N-terminal acetylation and methionine oxidation were set as variable modifications. For protein validation, a false discovery rate (FDR) of 1% was allowed at peptide and protein level based on a target/decoy search. Label-free quantification (LFQ) was done with MaxQuant using a minimum of 2 razor unique peptides. Maxquant output proteinGroups.txt was considered for data analysis using intensities columns.

Homology searching and domain analyses

37 genomes of SAR eukaryotic supergroup were searched (Table PX2 Dataset-2. The sampling included 4 *Plasmodium* spp, 14 other Apicomplexans, 5 Dinoflagellates, 2 Chromerids, 5 Ciliates, 3 Rhizaria, 3 Stramenopiles and 1 Perkinsea), collected from publicly available sources on 12 July 2025 (PX2_Dataset-2). Orthologs of PfPX2 were identified using Basic Local Alignment Search Tool (BLAST) and HMMer searches; both of which were performed using the AMOEBAE workflow[62]. HMMer searches were conducted using HMM profile including potential positive orthologs of PfPX2 in the protein databases of the selected organisms. A forward hit was considered a true ortholog if the generated E-value was below 0.05 and the same query sequence (PF3D7_0704400/XP_001348977.1) was retrieved as the top reverse BLAST hit, with an E-value two orders of magnitude lower than the next non redundant hit, if present. BLAST and HMMer searches were conducted using (1) full length PF3D7_0704400 query, (2) PF3D7_0704400 without PX domain, and (3) Only PX domain. Partial sequences with only PX domain were removed from the analyses.

Domain analysis was carried out in Interpro[63]. Putative hits containing both PX domain towards N-terminal of protein and WD repeats were considered true orthologs. Interpro's domain identification is based on various annotation databases. Hits with WD repeats, WD40/YVTN repeat-like domain or/and WD40 repeat containing domain were classified as positive as these correspond to homologous superfamilies or classified differently in specific databases. MAFFT (v7.511)[64] was used to align orthologues for domain and motif visualization.

Data availability

The data supporting the findings of this study are available within the paper and are also available from the corresponding author upon request.

Received: 21 July 2025; Accepted: 17 September 2025
Published online: 22 October 2025

References

1. Corvera, S., D'Arrigo, A. & Stenmark, H. Phosphoinositides in membrane traffic. *Curr. Opin. Cell Biol.* **11**, 460–465. https://doi.org/10.1016/S0955-0674(99)80066-0 (1999).
2. Di Paolo, G. & De Camilli, P. Phosphoinositides in cell regulation and membrane dynamics. *Nature* **443**, 651–657. https://doi.org/10.1038/nature05185 (2006).
3. Balla, T. Phosphoinositides: Tiny lipids with giant impact on cell regulation. *Physiol. Rev.* **93**, 1019–1137. https://doi.org/10.1152/physrev.00028.2012 (2013).
4. Nasuhoglu, C. et al. Nonradioactive analysis of phosphatidylinositides and other anionic phospholipids by anion-exchange high-performance liquid chromatography with suppressed conductivity detection. *Anal. Biochem.* **301**, 243–254. https://doi.org/10.1006/abio.2001.5489 (2002).
5. Wengelnik, K., Daher, W. & Lebrun, M. Phosphoinositides and their functions in apicomplexan parasites. *Int. J. Parasitol.* **48**, 493–504. https://doi.org/10.1016/j.ijpara.2018.01.009 (2018).
6. Ebrahimzadeh, Z., Mukherjee, A. & Richard, D. A map of the subcellular distribution of phosphoinositides in the erythrocytic cycle of the malaria parasite Plasmodium falciparum. *Int. J. Parasitol.* **48**, 13–25. https://doi.org/10.1016/j.ijpara.2017.08.015 (2018).
7. Chandra, M. et al. Classification of the human phox homology (PX) domains based on their phosphoinositide binding specificities. *Nat. Commun.* **10**, 1528. https://doi.org/10.1038/s41467-019-09355-y (2019).
8. Tawk, L. et al. Phosphatidylinositol 3-phosphate, an essential lipid in Plasmodium, localizes to the food vacuole membrane and the apicoplast. *Eukaryot. Cell* **9**, 1519–1530. https://doi.org/10.1128/EC.00124-10 (2010).
9. Vaid, A., Ranjan, R., Smythe, W. A., Hoppe, H. C. & Sharma, P. PfPI3K, a phosphatidylinositol-3 kinase from Plasmodium falciparum, is exported to the host erythrocyte and is involved in hemoglobin trafficking. *Blood* **115**, 2500–2507. https://doi.org/10.1182/blood-2009-08-238972 (2010).
10. Jakob Birnbaum, S. S. et al. A Kelch13-defined endocytosis pathway mediates artemisinin resistance in malaria parasites. *Science* **367**, 51–59 (2020).
11. Mukherjee, A. et al. A Phosphoinositide-binding protein acts in the trafficking pathway of hemoglobin in the malaria parasite Plasmodium falciparum. *MBio* **13**, 0323921. https://doi.org/10.1128/mbio.03239-21 (2022).
12. Jonscher, E. et al. PfVPS45 is required for host cell cytosol uptake by malaria blood stage parasites. *Cell Host. Microbe.* **25**(166–173), 165. https://doi.org/10.1016/j.chom.2018.11.010 (2019).
13. WHO. World malaria report 2024: Addressing inequity in the global malaria response. (2024).
14. Bjorkman, A., Benn, C. S., Aaby, P. & Schapira, A. RTS,S/AS01 malaria vaccine-proven safe and effective?. *Lancet Infect. Dis.* **23**, e318–e322. https://doi.org/10.1016/S1473-3099(23)00126-3 (2023).
15. Menard, D. & Fidock, D. A. Accelerated evolution and spread of multidrug-resistant Plasmodium falciparum takes down the latest first-line antimalarial drug in southeast Asia. *Lancet Infect. Dis.* **19**, 916–917. https://doi.org/10.1016/S1473-3099(19)30394-9 (2019).
16. Liffner, B. et al. Atlas of Plasmodium falciparum intraerythrocytic development using expansion microscopy. *bioRxiv* https://doi.org/10.1101/2023.03.22.533773 (2023).
17. Bannister, L. H., Hopkins, J. M., Fowler, R. E., Krishna, S. & Mitchell, G. H. Ultrastructure of rhoptry development in Plasmodium falciparum erythrocytic schizonts. *Parasitology* **121**, 273–287. https://doi.org/10.1017/s0031182099006320 (2000).
18. Rudlaff, R. M., Kraemer, S., Marshman, J. & Dvorin, J. D. Three-dimensional ultrastructure of Plasmodium falciparum throughout cytokinesis. *PLoS Pathog.* **16**, 1008587. https://doi.org/10.1371/journal.ppat.1008587 (2020).
19. Healer, J., Crawford, S., Ralph, S., McFadden, G. & Cowman, A. F. Independent translocation of two micronemal proteins in developing Plasmodium falciparum merozoites. *Infect. Immun.* **70**, 5751–5758. https://doi.org/10.1128/IAI.70.10.5751-5758.2002 (2002).
20. Hallee, S., Boddey, J. A., Cowman, A. F. & Richard, D. Evidence that the Plasmodium falciparum protein sortilin potentially acts as an escorter for the trafficking of the rhoptry-associated membrane antigen to the rhoptries. *mSphere* https://doi.org/10.1128/mSphere.00551-17 (2018).
21. Hallee, S., Counihan, N. A., Matthews, K., de Koning-Ward, T. F. & Richard, D. The malaria parasite Plasmodium falciparum sortilin is essential for merozoite formation and apical complex biogenesis. *Cell Microbiol.* **20**, 12844. https://doi.org/10.1111/cmi.12844 (2018).
22. Abramson, J. et al. Accurate structure prediction of biomolecular interactions with AlphaFold 3. *Nature* **630**, 493–500. https://doi.org/10.1038/s41586-024-07487-w (2024).
23. Pettersen, E. F. et al. UCSF chimeraX: Structure visualization for researchers, educators, and developers. *Protein Sci.* **30**, 70–82. https://doi.org/10.1002/pro.3943 (2021).
24. Chahar, P. et al. Genome-wide collation of the Plasmodium falciparum WDR protein superfamily reveals malarial parasite-specific features. *PLoS ONE* **10**, 0128507. https://doi.org/10.1371/journal.pone.0128507 (2015).
25. Jain, B. P. & Pandey, S. WD40 repeat proteins: Signalling scaffold with diverse functions. *Protein J.* **37**, 391–406. https://doi.org/10.1007/s10930-018-9785-7 (2018).
26. Teasdale, R. D. & Collins, B. M. Insights into the PX (phox-homology) domain and SNX (sorting nexin) protein families: Structures, functions and roles in disease. *Biochem. J.* **441**, 39–59. https://doi.org/10.1042/BJ20111226 (2012).
27. Bravo, J. et al. The Crystal Structure of the PX Domain from p40phox bound to phosphatidylinositol 3-phosphate. *Mol. Cell* **8**, 829–839 (2001).
28. Cheng, G. & Lambeth, J. D. NOXO1, regulation of lipid binding, localization, and activation of Nox1 by the Phox homology (PX) domain. *J. Biol. Chem.* **279**, 4737–4742. https://doi.org/10.1074/jbc.M305968200 (2004).
29. Birnbaum, J. et al. A genetic system to study Plasmodium falciparum protein function. *Nat. Methods.* **14**, 450–456. https://doi.org/10.1038/nmeth.4223 (2017).
30. Salmon, B. L., Oksman, A. & Goldberg, D. E. Malaria parasite exit from the host erythrocyte: A two-step process requiring extraerythrocytic proteolysis. *Proc. Natl. Acad. Sci. U. S. A.* **98**, 271–276. https://doi.org/10.1073/pnas.98.1.271 (2001).
31. Absalon, S., Robbins, J. A. & Dvorin, J. D. An essential malaria protein defines the architecture of blood-stage and transmission-stage parasites. *Nat. Commun.* **7**, 11449. https://doi.org/10.1038/ncomms11449 (2016).
32. Ebrahimzadeh, Z. et al. A pan-apicomplexan phosphoinositide-binding protein acts in malarial microneme exocytosis. *EMBO Rep.* https://doi.org/10.15252/embr.201847102 (2019).
33. Roucheray, S., Narciso, M. R. & Richard, D. Characterization of the malaria parasite. *Microbiol. Spectr.* https://doi.org/10.1128/spectrum.03288-24 (2025).

34. Kimmel, J. et al. Gene-by-gene screen of the unknown proteins encoded on Plasmodium falciparum chromosome 3. *Cell Syst.* **14**, 9–23. https://doi.org/10.1016/j.cels.2022.12.001 (2023).
35. Mukherjee, A. et al. A phosphoinositide-binding protein acts in the trafficking pathway of hemoglobin in the malaria parasite Plasmodium falciparum. *MBio* https://doi.org/10.1128/mbio.03239-21 (2022).
36. Zhang, M. et al. Uncovering the essential genes of the human malaria parasite Plasmodium falciparum by saturation mutagenesis. *Science* https://doi.org/10.1126/science.aap7847 (2018).
37. Elsworth, B. et al. The essential genome of. *Science* **387**, eadq6241. https://doi.org/10.1126/science.adq6241 (2025).
38. Prommana, P. et al. Inducible knockdown of Plasmodium gene expression using the glms ribozyme. *PLoS ONE* **8**, 73783. https://doi.org/10.1371/journal.pone.0073783.s005 (2013).
39. Goldfless, S. J., Wagner, J. C. & Niles, J. C. Versatile control of Plasmodium falciparum gene expression with an inducible protein–RNA interaction. *Nat. Commun.* **5**(1), 1–8. https://doi.org/10.1038/ncomms6329 (2014).
40. Ouyang, S., Jia, B., Xie, W., Yang, J. & Lv, Y. Mechanism underlying the regulation of sortilin expression and its trafficking function. *J. Cell Physiol.* **235**, 8958–8971. https://doi.org/10.1002/jcp.29818 (2020).
41. Sloves, P. J. et al. Toxoplasma sortilin-like receptor regulates protein transport and is essential for apical secretory organelle biogenesis and host infection. *Cell Host Microbe* **11**, 515–527. https://doi.org/10.1016/j.chom.2012.03.006 (2012).
42. Henrici, R. C. et al. The Plasmodium falciparum artemisinin susceptibility-associated AP-2 adaptin mu subunit is clathrin independent and essential for schizont maturation. *MBio* https://doi.org/10.1128/mBio.02918-19 (2020).
43. Dell'Angelica, E. C. Clathrin-binding proteins: Got a motif? Join the network!. *Trends Cell Biol.* **11**, 315–318. https://doi.org/10.1016/s0962-8924(01)02043-8 (2001).
44. Brodsky, F. M. Diversity of clathrin function: New tricks for an old protein. *Annu. Rev. Cell Dev. Biol.* **28**, 309–336. https://doi.org/10.1146/annurev-cellbio-101011-155716 (2012).
45. Pieperhoff, M. S., Schmitt, M., Ferguson, D. J. & Meissner, M. The role of clathrin in post-Golgi trafficking in toxoplasma gondii. *PLoS ONE* **8**, 77620. https://doi.org/10.1371/journal.pone.0077620 (2013).
46. Miao, J. & Cui, L. (bioRxiv, 2024).
47. Krai, P., Dalal, S. & Klemba, M. Evidence for a Golgi-to-endosome protein sorting pathway in Plasmodium falciparum. *PLoS ONE* **9**, 89771. https://doi.org/10.1371/journal.pone.0089771 (2014).
48. Sabitzki, R. et al. Role of Rabenosyn-5 and Rab5b in host cell cytosol uptake reveals conservation of endosomal transport in malaria parasites. *PLoS Biol.* **22**, 3002639. https://doi.org/10.1371/journal.pbio.3002639 (2024).
49. Sever, S., Chang, J. & Gu, C. Dynamin rings: Not just for fission. *Traffic* **14**, 1194–1199. https://doi.org/10.1111/tra.12116 (2013).
50. Breinich, M. S. et al. A dynamin is required for the biogenesis of secretory organelles in toxoplasma gondii. *Curr. Biol.* **19**, 277–286. https://doi.org/10.1016/j.cub.2009.01.039 (2009).
51. McGovern, O. L., Rivera-Cuevas, Y., Kannan, G., Narwold, A. J. Jr. & Carruthers, V. B. Intersection of endocytic and exocytic systems in toxoplasma gondii. *Traffic* **19**, 336–353. https://doi.org/10.1111/tra.12556 (2018).
52. Zhou, H. C., Gao, Y., Zhong, X. & Wang, H. Dynamin like protein 1 participated in the hemoglobin uptake pathway of Plasmodium falciparum. *Chin. Med. J.* **122**, 1686–1691. https://doi.org/10.3760/cma.j.issn.0366-6999.2009.14.015 (2009).
53. Li, H. et al. Isolation and functional characterization of a dynamin-like gene from Plasmodium falciparum. *Biochem. Biophys. Res. Commun.* **320**, 664–671. https://doi.org/10.1016/j.bbrc.2004.06.010 (2004).
54. Eisenberg-Bord, M., Shai, N., Schuldiner, M. & Bohnert, M. A tether is a tether is a tether: Tethering at membrane contact sites. *Dev. Cell* **39**, 395–409. https://doi.org/10.1016/j.devcel.2016.10.022 (2016).
55. Henne, W. M. et al. Mdm1/Snx13 is a novel ER-endolysosomal interorganelle tethering protein. *J. Cell Biol.* **210**, 541–551. https://doi.org/10.1083/jcb.201503088 (2015).
56. Daher, W. et al. Lipid kinases are essential for apicoplast homeostasis in toxoplasma gondii. *Cell Microbiol.* **17**, 559–578. https://doi.org/10.1111/cmi.12383 (2015).
57. Milani, K. J., Schneider, T. G. & Taraschi, T. F. Defining the morphology and mechanism of the hemoglobin transport pathway in Plasmodium falciparum-infected erythrocytes. *Eukaryot. Cell* **14**, 415–426. https://doi.org/10.1128/EC.00267-14 (2015).
58. Trager, W. & Jensen, J. B. Human malaria parasites in continuous culture. *Science* **193**, 673–675 (1976).
59. Elmendorf, H. G. & Haldar, K. Identification and localization of ERD2 in the malaria parasite Plasmodium falciparum: separation from sites of sphingomyelin synthesis and implications for organization of the Golgi. *EMBO J.* **12**, 4763–4773 (1993).
60. Schofield, L. et al. A rhoptry antigen of Plasmodium falciparum contains conserved and variable epitopes recognized by inhibitory monoclonal antibodies. *Mol. Biochem. Parasitol.* **18**, 183–195 (1986).
61. Coley, A. M. et al. Rapid and precise epitope mapping of monoclonal antibodies against Plasmodium falciparum AMA1 by combined phage display of fragments and random peptides. *Protein Eng.* **14**, 691–698 (2001).
62. Barlow, L. D. *et al.* 431–452 (Springer US, Golgi: Methods and Protocols, 2022).
63. Blum, M. et al. InterPro: The protein sequence classification resource in 2025. *Nucleic Acids Res.* **53**, D444–D456. https://doi.org/10.1093/nar/gkae1082 (2025).
64. Katoh, K. & Standley, D. M. MAFFT multiple sequence alignment software version 7: Improvements in performance and usability. *Mol. Biol. Evol.* **30**, 772–780. https://doi.org/10.1093/molbev/mst010 (2013).
65. Jones, P. et al. InterProScan 5: Genome-scale protein function classification. *Bioinformatics* **30**, 1236–1240. https://doi.org/10.1093/bioinformatics/btu031 (2014).

Acknowledgements

We would like to thank Maria R. Narciso and Roberto Botelho for discussions on PIP binding, Tobias Spielman for the SLI and KS plasmids and Michael Blackman and Alan Cowman for antibodies. We also thank Jacobus Pharmaceuticals for WR99210. The following reagents were obtained through MR4 as part of the BEI Resources, National Institute of Allergy and Infectious Diseases, National Institutes of Health, USA: Polyclonal Anti-Plasmodium falciparum PfERD2 (antiserum, Rabbit),). We would also like to acknowledge the Canadian Blood Services for providing human erythrocytes. UCSF ChimeraX, developed by the Resource for Biocomputing, Visualization, and Informatics at the University of California, San Francisco, with support from National Institutes of Health R01-GM129325 and the Office of Cyber Infrastructure and Computational Biology, National Institute of Allergy and Infectious Diseases. This study was funded through a Canadian Institutes for Health Research project grant (406675) to DR. DR was a Fonds de la Recherche du Québec-Santé Senior fellow. Research in the Dacks Lab is supported by the Natural Sciences and Engineering Research Council of Canada (RES0043758, and RES0046091). Research in the Griac laboratory is supported by the Scientific Grant Agency of the Ministry of Education, Research, Development, and Youth of the Slovak Republic and the Slovak Academy of Sciences grant VEGA 2/0047/23.

Author contributions

SR performed experimental work, interpreted results and edited the manuscript. DS, HK and DT performed

experimental work and interpreted results. JBD and PT designed experiments. DR conceived the study, designed experiments, interpreted results and wrote the manuscript.

Funding
This study was funded through a Canadian Institutes for Health Research project grant (406675) to DR. DR was a Fonds de la Recherche du Québec-Santé Senior fellow. Research in the Dacks Lab is supported by the Natural Sciences and Engineering Research Council of Canada (RES0043758, and RES0046091). Research in the Griac laboratory is supported by the Scientific Grant Agency of the Ministry of Education, Research, Development, and Youth of the Slovak Republic and the Slovak Academy of Sciences grant VEGA 2/0047/23. The funders had no role in the study.

Declarations

Competing interests
The authors declare no competing interests.

Additional information
Supplementary Information The online version contains supplementary material available at https://doi.org/10.1038/s41598-025-20974-y.

Correspondence and requests for materials should be addressed to D.R.

Reprints and permissions information is available at www.nature.com/reprints.

Publisher's note Springer Nature remains neutral with regard to jurisdictional claims in published maps and institutional affiliations.